Modelling the CO_2 mixing ratio with a mixed-layer model during day- and night-time conditions

Thirza van Laar

January 2014

Internship at Universitat Politecnica de Catalunya (UPC)
Advisor: David Pino (UPC)
Supervisor: Jordi Vila (Wageningen University)

Abstract

Previous research on the temporal evolution of CO_2 concentrations focused either on short, local time-scales, or on larger regional time-scales. On these different time-scales the importance of dynamical processes for the CO_2 concentration can differ as well. To study this shift of significance, a model is needed that is able to capture all relevant processes for both short and long time-scales.

The purpose of this paper is to extend a mixed-layer model in order to make it suitable for longer time-scales. A mixed-layer model is only valid for convective day-time conditions and can only simulate the convective boundary layer during several hours. By including the theory of Nappo & van Dop (1994) the model will also be suitable for simulating night-time conditions of the mixing ratio of CO_2, and as a consequence also longer simulations can be done with it.

The results of this extended model are compared with observations of 24-26 September 2003 to assess the accuracy. This shows that the mixing ratio of CO_2 is well captured during the first day and night, but after the transition of night to day the mixing ratio is too low. This is due to incorrect morning conditions (especially the boundary-layer depth), which emphasizes that when modelling the concentration of a chemical compound accurately, first the dynamical characteristics should be correct.

1 Introduction

In the context of global warming, it is important to be able to understand the evolution of carbon dioxide (CO_2) concentrations in the atmospheric boundary layer (ABL) and the factors that influence this evolution (Houghton, 1993; Cox *et al.*, 2000). It is already clear that next to processes at the surface, such as respiration and photosynthesis (Jacobs & de Bruin, 1992; Kim & Verma,

1990), also processes related to boundary layer dynamics have a large effect on the variability of CO_2 concentrations. Culf *et al.* (1997), as well as de Arellano *et al.* (2004) showed that during morning hours the CO_2 budget is more influenced by entrainment than by the surface flux. Casso-Torralba *et al.* (2008) assessed the importance of advection. With the help of a mixed-layer model, Pino *et al.* (2012) and Pino *et al.* (2013) studied how uncertainties in boundary layer dynamical variables influence the mixing ratio of CO_2. All in all, diurnal variability of CO_2 concentrations on local scales is quite well understood.

However, not only local spatial scales are of interest, but larger regional scales are that as well (Bakwin *et al.*, 2004). Increasing spatial scales automatically implies also increasing the time-scale of the processes involved (Stull, 2009). Certain dynamical processes are important on small time-scales, but they may loose their significance if the time-scale increases (Williams *et al.*, 2011). Entrainment and storage are usually ignored on time-scales larger than a day (Helliker *et al.*, 2004); on shorter time-scales it is common to neglect advection (Yi *et al.*, 2004). To study this shift in the importance of dynamical processes on CO_2 concentrations during the transition from local to regional scales, a model which is capable of capturing all dynamical processes involved, on increasing temporal scales, must be used. An example of such a model is the mixed-layer (MXL) model (Tennekes, 1973), which solves boundary layer dynamics together with atmospheric chemistry at low computational costs. However, this model is only valid for day-time conditions since it is based on the assumption of a convective, well-mixed boundary layer. It can therefore only be used for simulations up to several hours.

Because of this limitation of the MXL model, the purpose of this paper is to extend the model in such a way that it can also capture the evolution of CO_2 concentrations during stable conditions. By including the proposed algorithm of Nappo & van Dop (1994) for a scalar (in our case CO_2) for night-time conditions the simplicity of the model is kept. Nappo & van Dop (1994) show that their parameterization is mass conserving and gives realistic results for a scalar, when tested with a simple one-dimensional model.

After including their method, the extended model is suitable for longer simulations for the mixing ratio of CO_2 and we can increase the time-scale from hours to days. To assess the accuracy of the model, the results will be compared with observations, taken at Cabauw (The Netherlands) during three days: 24-26 September, 2003.

In the next section the theory for both the convective and the stable boundary layer on which the model is based will be described. Followed in section 3 by an analysis of the observations. In section 4 the settings of the model are given with which the results of section 5 are achieved. All this is summarized in the last section, where also the conclusions and an outlook to further research is given.

2 Theory

In this section the mixed-layer model is briefly described. It will be used to model the boundary layer variables during the day, in convective conditions. Next to the mixed-layer model, also the model used for the temporal evolution of the CO_2 mixing ratio during the night, when a stable layer has developed, is described in more detail. Finally, the methods for the transitions between these two different models are explained as well.

2.1 Convective Boundary Layer

Daytime conditions will be simulated by using zeroth-order mixed-layer theory (Tennekes, 1973; Tennekes & Driedonks, 1981; Driedonks, 1982). More recently models based on this theory has been used for example by de Arellano *et al.* (2004) to study the role of entrainment in the evolution and distribution of CO_2 in the boundary layer, and by Ouwersloot *et al.* (2012) to study the role of large scale atmospheric dynamics on the evolution of chemical species concentrations over a boreal forest.

During the day the boundary layer is assumed to be well mixed up to the thermal inversion due to turbulent mixing. This creates a vertically homogeneous profile of the mixing ratio of a conserved scalar in the boundary layer. The mixing ratio vertical profile of a conserved scalar shows a jump at the height of the inversion and above this height, in the free troposphere, the scalar mixing ratio follows a linear profile.

2.2 Stable Boundary Layer

During the night, radiative cooling at the surface produces a stable boundary layer (SBL), due to thermal stratification. Consequently, turbulence intensity is lower than during the day because it is only produced by mechanical mixing due to wind speed, producing less mixing during the night (Stull, 2009). In this situation mixed-layer theory is no longer valid. Due to the negative sensible heat flux and the consequential absence of vertical turbulent motions, it is assumed that there is no entrainment of CO_2 at the top of the boundary layer. Since the surface flux of CO_2 is positive during night time, mixing ratios are assumed to decrease linearly with height in the stable boundary layer.

To describe the boundary layer profile of CO_2 during night-time conditions in the model, the method described by Nappo & van Dop (1994) for the stable boundary layer is followed. It is important to note that this method doesn't analyse the atmospheric dynamics during the night, but only the scalar concentration. As in their theory we assume a constant nocturnal boundary-layer depth (z_i) and due to the absence of entrainment also a constant mixing ratio

of CO_2 at this height. Therefore, the CO_2 mixing ratio at a given height and time is represented by:

$$CO_2(z,t) \;=\; CO_{2,0}(t)\left(1-\frac{z}{z_i}\right)+CO_{2,z_i}\left(\frac{z}{z_i}\right) \tag{1}$$

where $CO_{2,0}$ is the mixing ratio at the surface, z the height and CO_{2,z_i} the mixing ratio of CO_2 at the boundary layer height. Different than Nappo & van Dop (1994), who dealt with a general atmospheric compound, we assume for our case that both the deposition flux and the source term of CO_2 (v_d and q_v in their equation 19) are zero. Therefore, $CO_{2,0}$ is given by:

$$CO_{2,0}(t) \;=\; CO_{2,z_i}+\frac{2\langle\overline{w'CO_2'}|_s\rangle}{z_i}(t-t_0), \tag{2}$$

where the averaged surface flux of CO_2, $\langle\overline{w'CO_2'}|_s\rangle$, is:

$$\langle\overline{w'CO_2'}|_s\rangle \;=\; [\int_{t_0}^{t}\overline{w'CO_2'}|_s\,\mathrm{d}t]/(t-t_0). \tag{3}$$

2.3 Transitions between day and night

To apply the equations of the previous subsections we assume that the transitions between day and night will occur when the sensible heat flux changes sign. The sensible heat flux is used for this since it is closely related to temperature and thereby to stability, regardless of the moisture conditions of the surface.

Because the stable boundary layer is shallower than the convective boundary layer (CBL), the profile of the CBL at the end of the day can be used as initial profile for the SBL. We assume a constant nocturnal boundary-layer depth and prescribe it by using the observations. Below that height the stable boundary layer develops. Above this height a residual layer is formed which remains unchanged during the night and has the same characteristics as the former CBL (Stull, 2009).

The transition from night to day is not as straightforward. The model should conserve the mass of CO_2, and the linearly decreasing profile must be converted into a vertically homogeneous one. On top of these restrictions there is also a residual layer left from the previous night. Ouwersloot *et al.* (2012) showed an example of how to deal with a residual layer in the mixed-layer model. However, if we would apply their same method, new initial values for the thermodynamical variables should be prescribed since they are not simulated during the night. To avoid this and to have a model that runs continuously, the residual layer is instantaneously incorporated in the mixed layer during the early morning. The height of the SBL is changed to the final height of the CBL of the previous day. The jump in the mixing ratio of

CO_2 at the boundary layer height and the CO_2 mixing ratio in the boundary layer itself are determined by guaranteeing mass conservation of CO_2. The gained mass of CO_2 during the night is evenly distributed over the new, higher boundary-layer depth.

3 Observations

By using observations we describe the evolution of the boundary layer dynamics and the CO_2 mixing ratio during the period of 24-26 September 2003, with a special interest in the nights. The day of 25 September has already been studied by Casso-Torralba *et al.* (2008) and Pino *et al.* (2012). Observations are from the Cabauw site (The Netherlands), which is surrounded by an open field mostly covered with short grass. Beljaars & Bosveld (1997) and Vermeulen *et al.* (2011) described the measurement site in detail. Along the 213-m meteorological tower of this site the vertical profiles of temperature, humidity, wind and CO_2 are measured, as well as the fluxes of momentum, CO_2, sensible and latent heat. The CO_2 mixing ratio is measured at 20, 60, 120 and 200 m, the flux of CO_2 is measured at 5, 60, 100 and 180 m.

3.1 Temporal evolutions

Figure 1 shows the temporal evolution at all available measurement heights of potential temperature, wind speed and the CO_2 mixing ratio for both nights of interest. For the same period, Figure 2 shows the temporal evolution of the flux of CO_2, the sensible and latent heat flux at 5, 60, 100 and 180 m.

The potential temperature decreases in the lower layers (up to 40/80 m for night 1/2, Figs. 1-a,b), and this cooling produces a stable layer. This is confirmed by the negative sensible heat fluxes, which can be observed in Figures 2-a,b. The time of the minimum sensible heat flux differs between the two nights. Steeneveld *et al.* (2005) found a coupling between the heat fluxes and wind speed, and we can find it here as well. The wind speeds are shown in Figs. 1-c,d. In the first night wind speed increases gradually to a maximum at the end of the night, also the fluxes have their largest magnitude at the end of the night. In the second night the maximum wind speed is found at the beginning of the night. This can explain the sudden variations of the fluxes during the second night at 21 UTC.

Because of respiration by the soil and by vegetation, CO_2 mixing ratio increases during the night (Figs. 1-e,f). At the end of both nights the mixing ratio of CO_2 at 20 m reaches a value of approximately 440 ppm. This represents an increase of 60 ppm and 50 ppm for the first and second night respectively. The time of the maximum CO_2 mixing ratio for the two lowest levels coincides

with the largest observed CO_2 fluxes at the surface (Figs. 2-e,f).

By analysing observations taken during the first night (Figs. 1-a,c,e) it is noticed that there is a decoupling between 40 and 80 m. Above 80 m the temperature does not increase anymore, staying fairly constant. In the tendency of wind speed and CO_2 for this night (Figs. 1-a,e) the same decoupling is seen, from which can be deduced that the stable boundary-layer depth must be in the range of 40-80 m for the first night. For the second night (Figs. 1-b,d,f), this decoupling is observed between 80 and 140 m. Thus the stable boundary layer becomes not as shallow in the second night as in the first night. Unfortunately there is no continuous data of night-time boundary-layer depths available to verify this.

3.2 Radiosondes

Figure 3 shows three vertical profiles of potential temperature (θ) as observed by radiosondes on 24 and 25 September at 12 UTC and on 25 September at 00 UTC. The radiosondes are launched at De Bilt, approximately 40 km away from Cabauw. The well-mixed profiles for potential temperature during the day are clearly visible. Unfortunately the sounding of 26 September at 00 UTC did not record data below 200 m. The launch on 25 September at 00 UTC shows the linearly increasing profile of potential temperature during the night. It can also be seen that the boundary-layer depth is located at least lower than 100 m for this night.

3.3 Budget analysis

By using the observations shown in Figures 1,2, the budget analysis method can be applied (Betts, 1992; Betts & Ball, 1994; de Arellano *et al.*, 2004). With this method the contribution of advection, vertical flux divergence and storage for a scalar can be assessed. Notice that radiative cooling is not included, and since this is an important process influencing temperature during the night, the method cannot be applied for this variable during the night. Due to the relative homogeneous surface conditions at Cabauw, the horizontal flux divergence is omitted for this study. Next to this and following de Arellano *et al.* (2004) and Casso-Torralba *et al.* (2008) the vertical advection is omitted as well. The budget for a scalar S then reads:

$$\frac{\partial \overline{S}}{\partial t} + \overline{u}\frac{\partial \overline{S}}{\partial x} + \overline{v}\frac{\partial \overline{S}}{\partial y} + \frac{\partial \overline{w'S'}}{\partial z} \approx 0 \tag{4}$$

In this equation the first term represents the storage term (or tendency term) and is expressed as the rate of change of the scalar in time. The second and third terms are the horizontal advection. Finally, the last term represents the

divergence of the scalar flux which accounts for the vertical transport of the scalar.

The storage term is determined by using the average value of observations at 60 and 20 m. These heights are different than for example in the study of Casso-Torralba *et al.* (2008). This is because we analyse the stable boundary layer instead of the convective boundary layer and the heights of the observations have to be in the boundary layer (Betts, 1992). The same holds for the determination of the divergence of the CO_2 flux. For this, the observations at 60 and 5 m are used, so that both are very likely to be inside the nocturnal boundary layer. Unfortunately, there is no data available from the same heights as for the storage term. The horizontal advection is assumed to be the residual term of the equation when storage and divergence are known.

The result for the CO_2 budget for both nights is shown in Fig. 4. During both nights storage is a positive term, as could already be deduced by the increasing mixing ratios in Figs. 1-e,f. Note that due to the sign convention used here, negative advection means air rich(er) in CO_2. The storage of CO_2 at the end of both nights has comparable magnitude (4 ppm/hour). This is supported by Figs. 1-e,f, showing that the CO_2 mixing ratio at the surface at the end of both nights reaches approximately the same value (440 ppm). However, although the total storage of both nights is comparable, this is not the case for the divergence of the CO_2 flux and advection. In the first night the divergence of the CO_2 flux is close to zero, whereas in the second night it reaches a value of -1.5 ppm/hour. At the same time the advection is less negative (so less advection of CO_2), leading to comparable storage terms for both nights.

4 Model settings

Table 1 shows the initial settings used for the simulation. They are based on the observations shown in the previous section. Note that we assume that there is no advection. The prescribed fluxes of sensible heat, latent heat and CO_2 follow a sinusoidal function during both day and night and are fitted by using the observations of the fluxes at 5 m, as illustrated in Fig. 5. The magnitude of their maxima and minima can be found in Table 2.

The simulation starts at 8 UTC in the morning of 24 Sep and ends at 16 UTC on 26 Sep. The start and end times of the nights (moments of transition) are shown in Table 3.

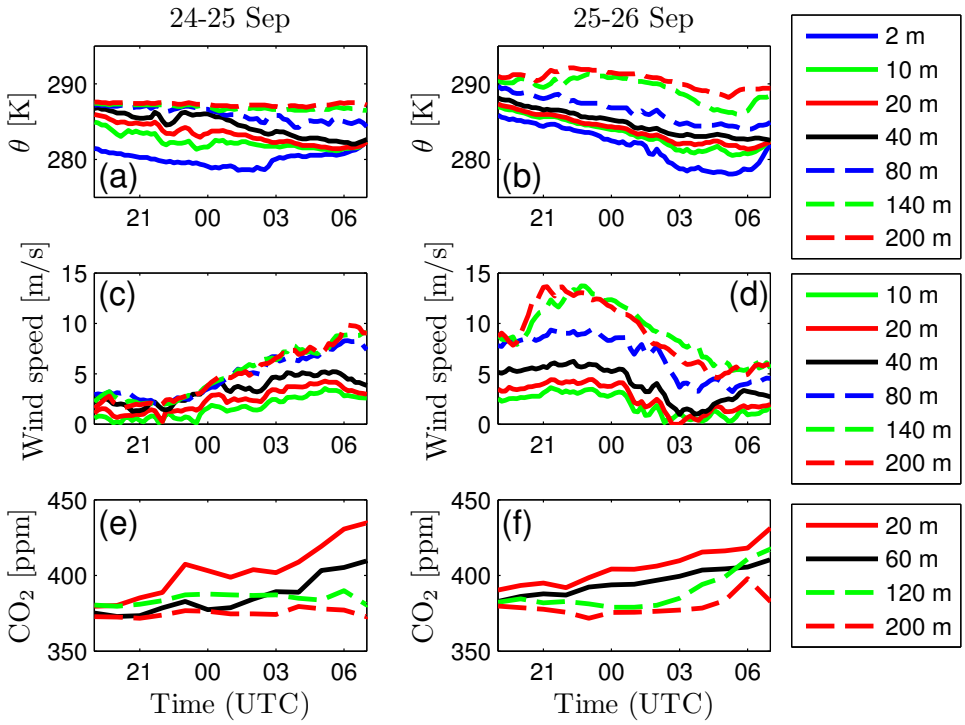

Figure 1: Temporal evolution of the observed potential temperature (a,b), wind speed (c,d) CO_2 mixing ratio (e,f), at all available measurement heights for the nights of 24-25 and 25-26 September 2003.

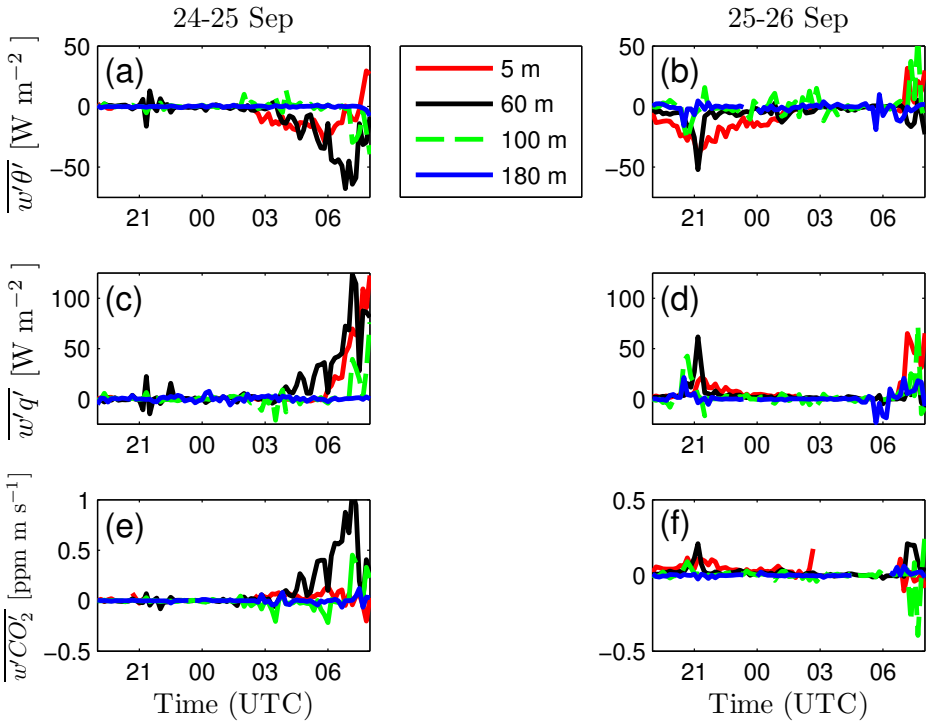

Figure 2: Temporal evolution of the observed fluxes of sensible heat (a,b), latent heat (c,d) and CO_2 (e,f) for the nights of 24-25 and 25-26 September 2003.

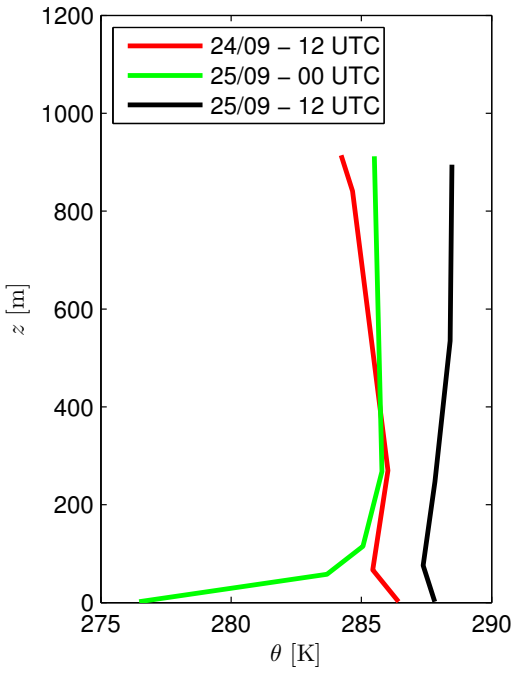

Figure 3: Observed vertical profile of potential temperature on 24 and 25 Sep at 12 UTC, and on 25 Sep at 00 UTC.

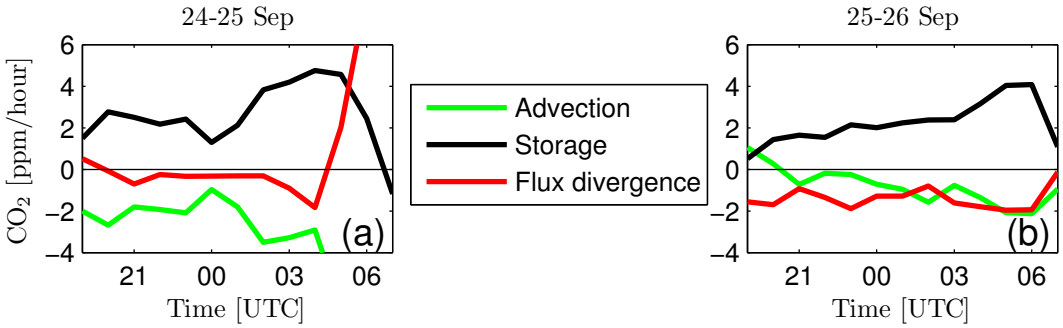

Figure 4: Temporal evolution of the CO_2 budget (see Eq. 4) on 24-25 (a) and 25-26 (b) September.

Table 1: Initial (subscript 0) and prescribed values as used for the simulation of three days (24-26 Sep) based on the observations taken at Cabauw. z_i is the boundary-layer depth, w_s is the subsidence velocity and β is the entrainment ratio. The jump of the scalars i is represented by Δi and the lapse rate in the free troposphere is given by γ_i.

$z_{i,0}$ (m)	80
w_s (m/s)	0
β	0.3
θ_0 (K)	284.5
$\Delta\theta$ (K)	3.5
γ_θ (K/m)	0.0035
q_0 (g/kg)	4.3
Δq (g/kg)	-0.8
γ_q (g/kg m)	-0.002
$CO_{2,0}$ (ppm)	400
ΔCO_2 (ppm)	-28
γ_{CO_2} (ppm/m)	-0.003
z_i, first night (m)	60
z_i, second night (m)	100

Table 2: Magnitude of the maxima and minima of the prescribed fluxes used in the model. All fluxes follow a sinusoidal function during both day and night and are fitted through the observations.

	24 Sep	24-25 Sep	25 Sep	25-26 Sep	26 Sep
$\overline{w'\theta'}\|_s$ (K m s^{-1})	0.064	-0.02	0.081	-0.02	0.081
$\overline{w'q'}\|_s$ (g kg^{-1} m s^{-1})	0.083	0.0	0.078	0.0	0.058
$\overline{w'CO_2'}\|_s$ (ppm m s^{-1})	-0.18	0.07	-0.1	0.07	-0.02

Table 3: Times of the night-time conditions for the sensible heat flux, latent heat flux and the flux of CO_2, respectively.

	24-25 Sep	25-26 Sep
$\overline{w'\theta'}\|_s$	16:30-08:00	16:00-08:00
$\overline{w'q'}\|_s$	17:00-07:00	18:00-08:00
$\overline{w'CO_2'}\|_s$	16:00-07:30	16:00-08:00

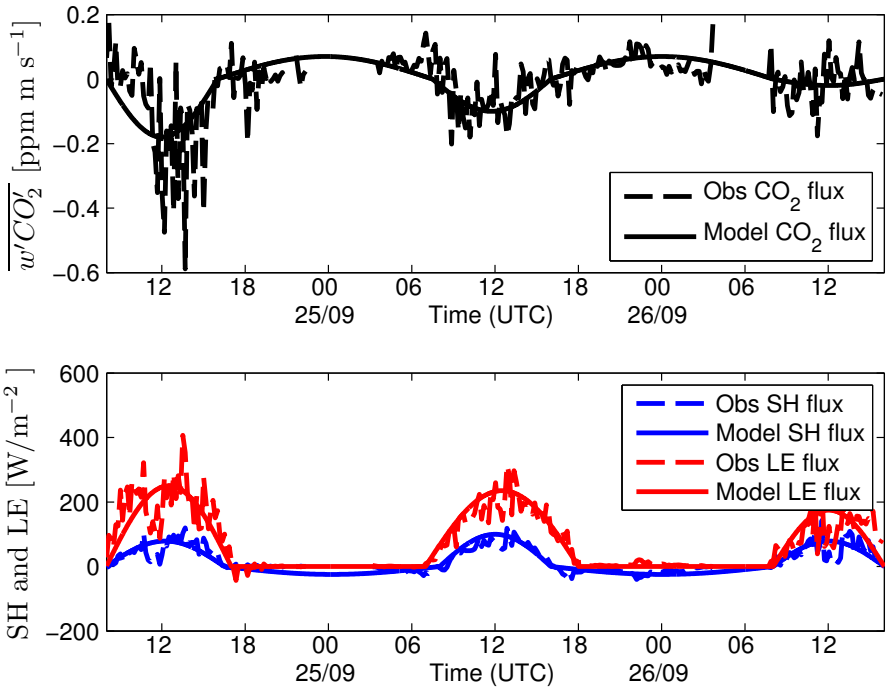

Figure 5: (a) Temporal evolution of the CO_2 flux, measured at 5 m above ground level (dashed line). The solid line represents the prescribed surface fluxes of CO_2 used in the mixed layer model. (b) Temporal evolution of the sensible (SH, blue dashed line) and latent heat fluxes (LE, red dashed line) at 5 m. The solid blue and red line represent the prescribed sensible and latent heat flux of the model respectively.

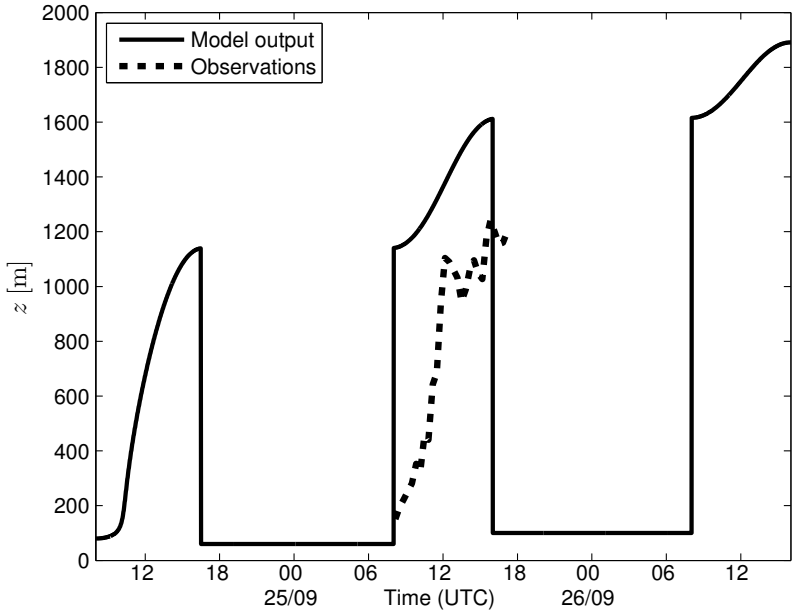

Figure 6: Temporal evolution of the observed (dots) and simulated by the model (solid line) boundary-layer depth for the three studied days.

5 Results

With the model set up presented in the previous section a simulation of three days is performed. First the temporal evolution of the boundary-layer depth is analysed. This is followed by an analysis of the temporal evolution of the CO_2 mixing ratio.

5.1 Boundary-layer depth

Figure 6 shows the temporal evolution of the boundary layer depth for the three days of the simulation, starting on 24 September 2003 at 8 UTC. Only observations of 25 September are available, showing that the model overestimates the boundary-layer depth during the second day. This is due to the estimation of the boundary-layer depth at the start of the day, caused by the assumptions made for the transition from night to day. If the correct morning initial conditions are used, the boundary-layer depth would be well represented (see Pino *et al.* (2012)). By including the method of Ouwersloot *et al.* (2012) for the residual layer, the results will improve.

5.2 Temporal evolution of the CO_2 mixing ratio

Figure 7 shows the temporal evolution of the CO_2 mixing ratio for the total period of the simulation. The blue, solid line represents the CO_2 mixing ratio as solved by the model at 20 m. For the first day and night mixing ratios are well reproduced, confirming the model proposed by Nappo & van Dop (1994). During the night mixing ratios are increasing with a comparable slope as the observations, only the maximum mixing ratios at the end of the night are underestimated. Some possible reasons for this can be a wrong boundary-layer depth, or the presence of advection, which was neglected in the model.

At the start of the second day there is a sudden decrease of the modelled CO_2 mixing ratio at the time of the transition between night and day. This is because the boundary layer suddenly jumps back to the height it had at the end of the previous day, instead of growing steadily during the day. The large boundary layer causes a low CO_2 mixing ratio, and since the boundary-layer depth during this day stays too large (see previous subsection and Fig. 6), the mixing ratios during this day stay too low. This fact causes wrong initial conditions for the start of the second night, and therefore the model underestimates CO_2 mixing ratios during this night. Figure 8 shows the temporal evolution of CO_2 for a simulation which starts at 25 September to ensure correct initial conditions at the beginning of that day. For this simulation the same settings as in Pino *et al.* (2012) are used. The run starts at 8 UTC on 25 September and ends at 16 UTC on 26 Sep. The same times and magnitudes for the fluxes of heat and CO_2 are used as in the simulation for three days (Tables 2,3).

As can be seen in Fig. 8, the day and night of 25 Sep are both well represented if the dynamical, initial conditions are correct. Although again the maximum mixing ratio at the end of the night is not correctly captured by the model.

6 Summary and Conclusions

The purpose of this paper is to extend the mixed-layer model to be able to simulate CO_2 mixing ratios for several days. This is done by incorporating the theory of Nappo & van Dop (1994) for stable conditions to a mixed-layer model. The extended model is used for a simulation of three days with initial conditions and external forcings based on the observations of 24-26 September 2003.

The observations of the nights on 24-25 and 25-26 September show, as expected, that the potential temperature decreases and CO_2 mixing ratio increases with height. From the observations can be concluded that the boundary layer is slightly higher in the second night than in the first night. The CO_2

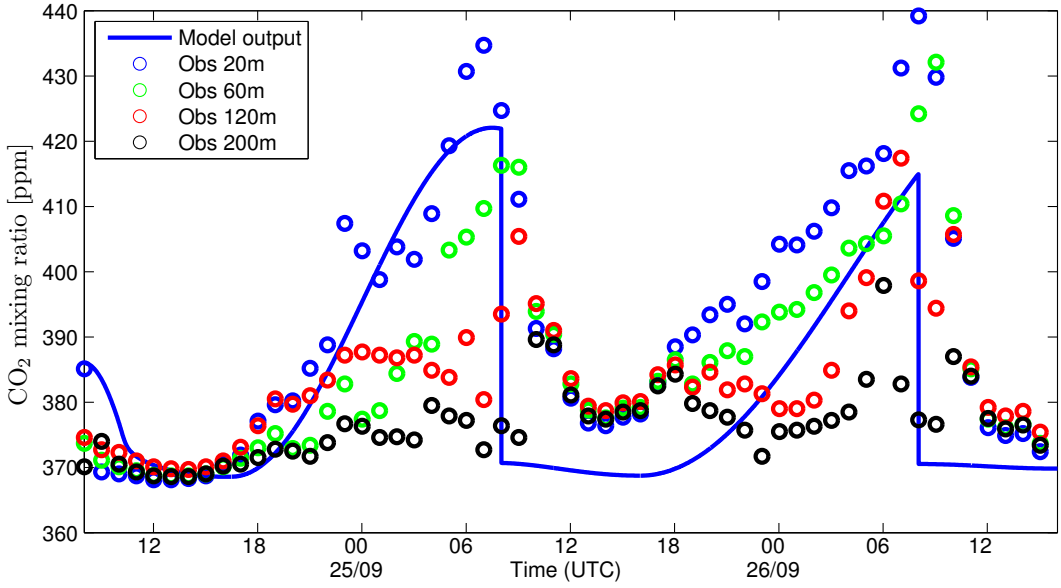

Figure 7: Temporal evolution of the observed (dots) and simulated at 20 m (solid line) CO_2 mixing ratio for the three studied days.

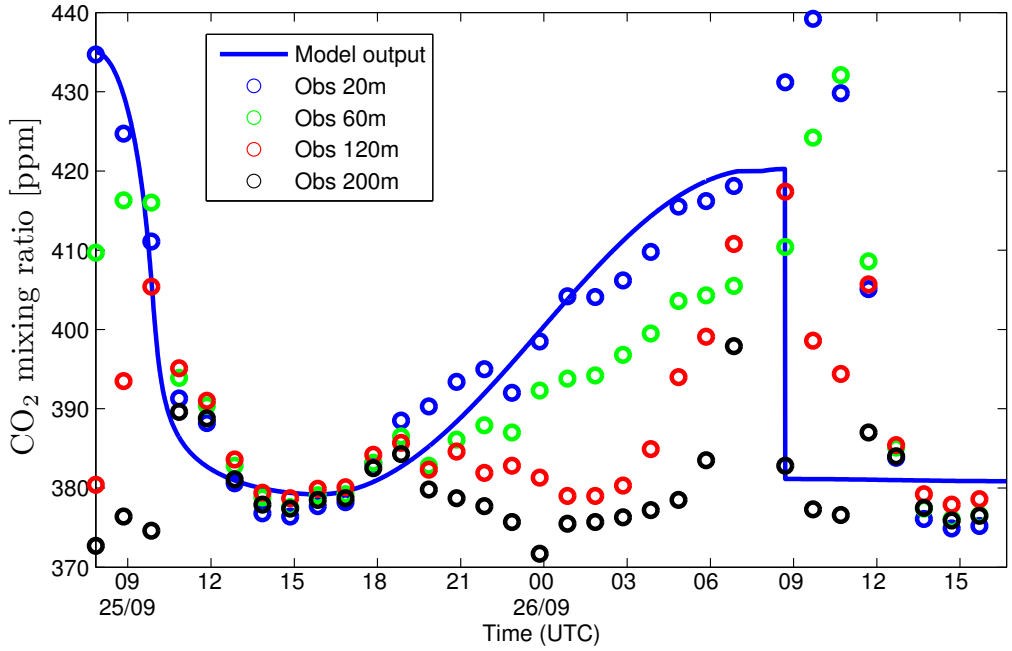

Figure 8: Temporal evolution of the observed (dots) and simulated at 20 m (solid line) CO_2 mixing ratio when the model is initialized at 8 UTC on 25 September 2003.

mixing ratios are comparable for both nights, although during the first night advection plays a more important role than during the second night. Unfortunately there is only one radiosonde launched during night-time available (00 UTC, 25 Sep), it shows that the potential temperature profile linearly increases with height.

During the first day the model correctly reproduces the atmospheric dynamics. This leads also to correct CO_2 mixing ratios. Also the CO_2 mixing ratios during the first night are well represented, confirming the theory of Nappo & van Dop (1994). However, due to an oversimplification of the night-day transition, the morning value of the boundary-layer depth for the second day is incorrect. This leads to an overestimation of the boundary-layer depth and therefore too low mixing ratios for CO_2 during the rest of the simulated period.

We can conclude that, although several assumptions were made, the CO_2 mixing ratios of the first night are well reproduced by the model. Nevertheless, for simulations longer than one day it is necessary to improve the method for the transition between night and day, thereby providing correct dynamical conditions at the start of the day.

Once the transition from night to day is improved the model might be suitable for increasing the time-scale. It then can be used in a sensitivity analysis to study the contribution of different processes influencing the CO_2 mixing ratio on increasing time-scales, thereby bridging the gap between local and regional scale models.

References

Bakwin, P. S., Davis, K. J., Yi, C., Wofsky, S. C., Munger, J. W., Haszpra, L., & Barcza, Z. 2004. Regional carbon dioxide fluxes from mixing ratio data. *Tellus*, **56B**, 301–311.

Beljaars, A.C.M., & Bosveld, F.C. 1997. Cabauw data for the validation of land surface parameterization schemes. *J. Clim.*, **10**, 1172–1193.

Betts, A.K. 1992. FIFE Atmospheric Boundary Layer Budget Methods. *J. Geophys. Res.*, **97**, 18,523–18,531.

Betts, A.K., & Ball, J.H. 1994. Budget analysis of FIFE 1987 Sonde Data. *J. Geophys. Res.*, **99**, 3655–3666.

Casso-Torralba, P., de Arellano, J. V.-G., Bosveld, F., Soler, M.R., Vermeulen, A., Werner, C., & Moors, E. 2008. Diurnal and vertical variability of the sensible heat and carbon dioxide budgets in the atmospheric surface layer. *J. Geophys. Res.*, **113**(D12).

Cox, PM, Betts, RA, Jones, CD, Spall, SA, & Totterdell, IJ. 2000. Acceleration of global warming due to carbon-cycle feedbacks in a coupled climate model. *Nature*, **408**, 184–187.

Culf, A.D., Fisch, G., Malhi, Y., & Nobre, C.A. 1997. The influence of the atmospheric boundary layer on carbon dioxide concentrations over a tropical forest. *Agricultural Forest Meteorol.*, **85**, 149–158.

de Arellano, J. V.-G., Gioli, B., Miglietta, F., Jonker, H. J. J., Baltink, H. K., Hutjes, R. W. A., & Holtslag, A. A. M. 2004. Entrainment process of carbon dioxide in the atmospheric boundary layer. *J. Geophys. Res.*, **109**.

Driedonks, A. G. M. 1982. Sensitivity analysis of the equations for a convective mixed layer. *Bound. Layer Meteorol.*, **22**, 475–480.

Helliker, B.R., Berry, J.A., Betts, A.K., Bakwin, P.S., Davis, K.J., Denning, A.S., Ehleringer, J.R., Miller, J.B., Butler, M.P., & Ricciuto, D.M. 2004. Estimates of net CO2 flux by application of equilibrium boundary layer concepts to CO2 and water vapor measurements from a tall tower. *J. Geophys. Res.*, **109**.

Houghton, J. 1993. The scientific basis for the prediction of climate change. *Int. J. Environ. Pollut.*, **3**.

Jacobs, C. M. J., & de Bruin, H. A. R. 1992. The sensitivity of regional transpiration to land-surface characteristics: Significance of feedback. *J. Clim.*, **5**, 683–698.

Kim, J., & Verma, S.B. 1990. Carbon dioxide exchange in a temperate grassland ecosystem. *Bound. Layer Meteorol.*, **52**, 135–149.

Nappo, C.J., & van Dop, H. 1994. Simple boundary layer description for global dispersion models. *J. Geophys. Res.*, **99**, 10527–10534.

Ouwersloot, H. G., de Arellano, J. V.-G., Nolscher, A. C., Krol, M. C., Ganzeveld, L. N., Breitenberger, C., Mammarella, I., Williams, J., & Lelieveld, J. 2012. Characterization of a boreal convective boundary layer and its impact on atmospheric chemistry during HUMPPA-COPEC-2010. *Atmos. Chem. Phys.*, **12**, 9335–9353.

Pino, D., de Arellano, J. V.-G., Peters, W., Schroter, J., van Heerwaarden, C. C., & Krol, M. C. 2012. A conceptual framework to quantify the influence of convective boundary layer development on carbon dioxide mixing ratios. *Atmos. Chem. Phys.*, **12**, 2969–2985.

Pino, D., Kaikkonen, J.P., & de Arellano, J. V.-G. 2013. Quantifying the uncertainties of advection and boundary layer dynamics on the diurnal carbon dioxide budget. *J. Geophys. Res. Atmos.*, **118**.

Steeneveld, G. J., van de Wiel, B. J. H., & Holtslag, A.A.M. 2005. Modeling the Evolution of the Atmospheric Boundary Layer Coupled to the Land Surface for Three Contrasting Nights in CASES-99. *J. Atmos. Sci.*, **63**, 920–935.

Stull, R.B. 2009. *An Introduction to Boundary Layer Meteorology.* Springer.

Tennekes, H. 1973. A Model for the Dynamics of the Inversion Above a Convective Boundary Layer. *J. Atmos. Sci.*, **30**, 558–567.

Tennekes, H., & Driedonks, A.G.M. 1981. Basic entrainment equations for the atmospheric boundary layer. *Bound. Layer Meteorol.*, **20**, 515–531.

Vermeulen, A. T., Hensen, A., Popa, M.E., van den Bulk, W.C.M., & Jongejan, P.A.C. 2011. Greenhouse gas observations from Cabauw Tall Tower (1992-2010). *Atmos. Meas. Tech.*, **4**, 617–644.

Williams, I. N., Riley, W. J., Torn, M. S., Berry, J. A., & Biraud, S. C. 2011. Using boundary layer equilibrium to reduce uncertainties in transport models and CO2 flux inversions. *Atmos. Chem. Phys.*, **11**, 96319641.

Yi, C., Davis, K.J., Bakwin, P.S., Denning, A.S., Zhang, N., Desai, A., Lin, J.C., & Gerbig, C. 2004. Observed covariance between ecosystem carbon exchange and atmospheric boundary layer dynamics at a site in northern Wisconsin. *J. Geophys. Res.*, **109**.